Feb, 1986

CONFINED COMPRESSIVE STRENGTH OF MULTI-YEAR PRESSURE RIDGE SEA ICE SAMPLES

C.F.N. Cox and J.A. Richter-Menge
U. S. Army Cold Regions Research and Engineering Laboratory
Hanover, New Hampshire, U.S.A.

ABSTRACT

Fifty-five constant-strain-rate triaxial tests were performed on vertically oriented multi-year pressure ridge samples from the Beaufort Sea. The tests were performed on a closed-loop electrohydraulic testing machine at two nominal strain rates (10^{-5} and 10^{-3} s^{-1}) and two temperatures (-20° and -5°C). In all of the tests the confining pressure was ramped in constant proportion to the applied axial stress ($\sigma_1 > \sigma_2 = \sigma_3$, σ_3/σ_1 = constant). Two σ_3/σ_1 ratios were investigated: 0.25 and 0.50. This paper summarizes the sample preparation and testing techniques used in this investigation and presents data on the confined compressive strength and failure strain of the ice. Uniaxial data are also included for comparison.

INTRODUCTION

Data on the mechanical properties of multi-year pressure ridges are needed to design safe, cost-effective structures in exposed areas of the Beaufort and Chukchi seas. Data are now available on the uniaxial compressive and tensile strength of ice samples from multi-year pressure ridges (1-5). However, ice-structure interaction processes generally result in a complex state of stress in the ice. Additional information on the confined compressive strength of the ice is required to develop constitutive equations to properly describe the interaction process. This paper presents data on the confined compressive strength and failure strain of ice samples from multi-year pressure ridges. The effects of ice structure, temperature, porosity, strain rate, and confining pressure on the test results are also examined.

ICE DESCRIPTION

The triaxial specimens tested in this program were derived from two multi-year pressure ridges in the Beaufort Sea, just northwest of Prudhoe Bay, Alaska. The test samples had an average salinity of 0.762 0.658‰ and an average density of 0.854 ± 0.037 Mg/m^3 at -20°C. Test specimen porosities varied from 17 to 203‰. All but seven of the samples contained various mixtures of granular and columnar grains. There was one columnar sample and six granular samples. Additional information on the salinity, density, and structure of ice samples from multi-year pressure ridges can be found in Richter and Cox (12) and Richter-Menge and Cox (13).

TEST METHODS

Fifty-five constant-strain-rate triaxial tests were performed on vertically oriented multi-year pressure ridge samples. The tests were conducted on a closed-loop electrohydraulic testing machine at two nominal strain rates (10^{-5} and 10^{-3} s^{-1}) and two temperatures (-20 and -5°C). In all of the tests the confining pressure was ramped in constant proportion to the applied axial stress ($\sigma_1 > \sigma_2 = \sigma_3$, σ_3/σ_1 = constant). Two σ_3/σ_1 ratios were investigated: 0.25 and 0.5.

Test specimens were prepared from 10.7-cm-diameter cores. Samples were first rough-cut on a band saw, and the ends were milled square on a milling machine to produce 25.4-cm-long test specimens. Synthane end caps were then bonded to the samples, and the samples were turned on a lathe to a slight dumbbell shape having a neck diameter of 10.2 cm. The form tool used to turn the specimens had a radius of curvature of 20.4 cm, twice the diameter of the finished neck. This radius was chosen to minimize stress concentrations near the sample end planes. Every effort was made to produce properly sized, precision-machined test samples utilizing recommended methods (6,7).

The design of the triaxial cell used at CRREL to investigate the mechanical properties of multi-year sea ice was suggested by Mellor (8). Unlike standard triaxial cells, the confining pressure in the CRREL cell was not maintained at a constant level; instead, it was ramped in constant proportion to the applied axial stress. This was accomplished by the use of a special intercylinder mounted in the loading train on top of the cell (Fig. 1). For a right cylindrical specimen, the ratio of the confining pressure to the axial stress

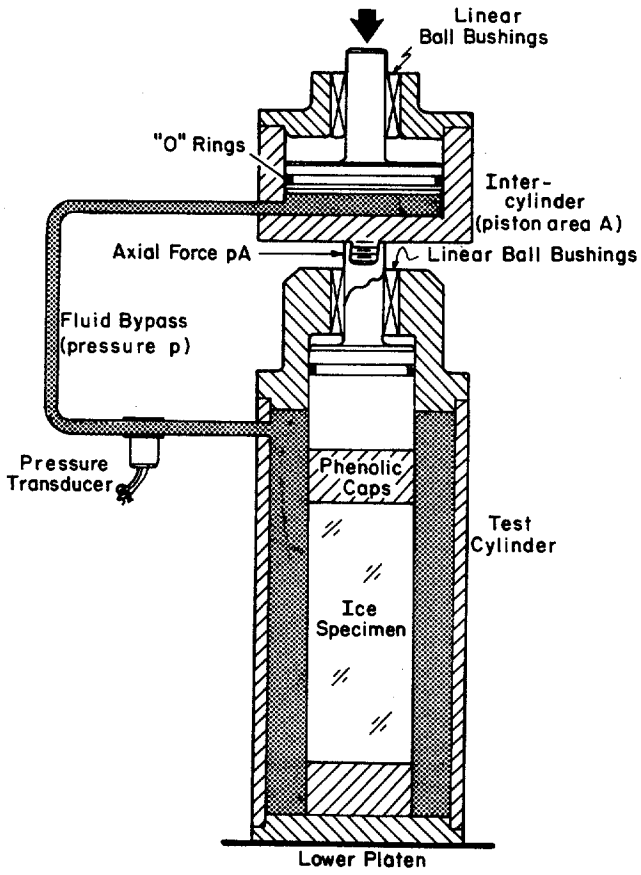

Fig. 1. Schematic diagram of triaxial cell.

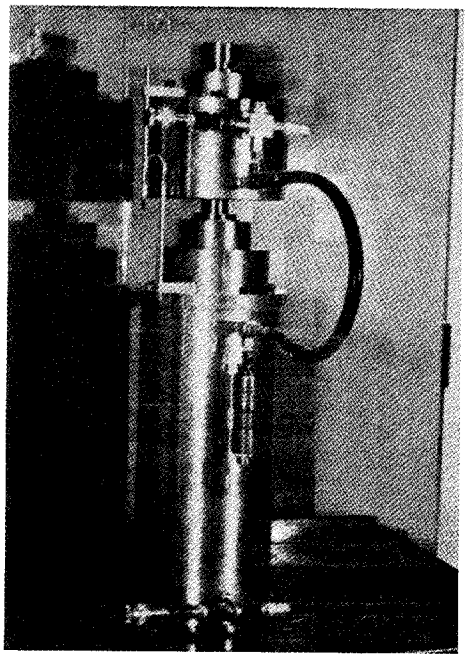

Fig. 2. Triaxial cell showing extensometer mounting rods on upper cylinder and top of cell.

was determined by the ratio of the diameter of the piston entering the cell (sample diameter) to the diameter of the piston in the upper intercylinder. The ratio was changed by inserting a reducing sleeve and new piston into the upper cylinder. To ensure that the proper σ_3/σ_1 ratio was obtained throughout each test, the fluid pressure was continuously monitored by a pressure transducer.

All of the tests were performed on a closed-loop electrohydraulic testing machine. The machine had two actuators with capacities of 1.1 and 0.11 MN and a fast response, high-flow-rate servo-valve. The load frame of the machine had a capacity of 2.2 MN. The 1.1 MN actuator was used for the triaxial tests.

Sample strains in most of the tests were measured and controlled with an extensometer mounted on U-shaped bars that were attached to the upper cylinder and cell as shown in Figure 2. Later in the test program, the method for measuring axial strains was improved. In the new set-up, the strain rate was controlled by monitoring the output from two extensometers mounted on the shaft going into the triaxial cell (Fig. 3). Some of the earlier test results indicated that the upper cylinder rotated slightly at the beginning of a test. In general it is good practice to measure as little of the loading train deformation as possible when transducers cannot be placed directly on the ice. Two transducers, mounted on opposite sides of the sample, are

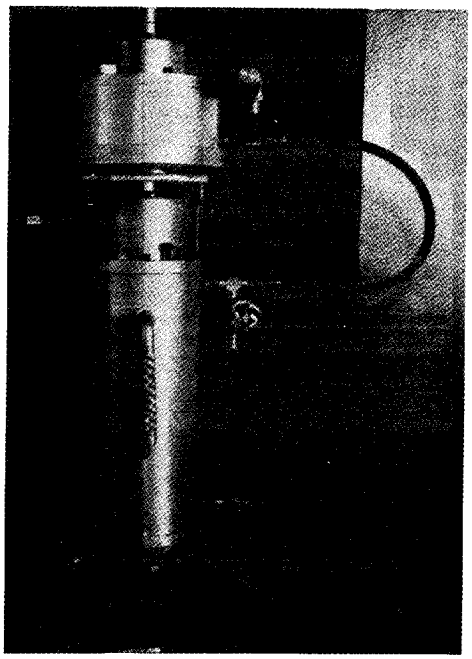

Fig. 3. Triaxial cell showing two extensometers mounted on shaft going into triaxial cell.

also desirable, as they provide a measure of the average axial sample displacement.

Test temperatures were controlled to within 0.5°C by placing the sample in an environmental chamber mounted between the columns of the testing machine. Load and sample strain rate data were recorded on an XY plotter, several strip charts, and a FM magnetic tape recorder. Detailed information on our sample preparation and testing techniques can be found in Mellor et al. (8) and Cox and Richter-Menge (9).

TEST RESULTS

Representative load-displacement curves from the triaxial tests are shown in Figure 4. Four kinds of behavior were observed and are designated as types A, B, C, and D. The type of behavior observed for each test condition is summarized in Table 1.

Originally it was assumed that the loading train and sample end caps were rigid. However, when the triaxial data were analyzed we found that the confined initial tangent modulus data were consistently lower than the initial tangent modulus of the uniaxial or unconfined specimens. This caused some concern because we would expect the confined modulus to be greater. Any confinement should reduce the axial displacement for a given load and thereby increase the measured modulus.

After checking our testing techniques and data reduction procedures, it was concluded that the lower confined modulus values were due to the use of the synthane end caps on our samples in the triaxial cell with externally mounted displacement transducers. In effect, because sample displacements were measured outside the triaxial cell, the synthane end caps became a compliant element in an otherwise stiff loading system. If displacements were measured on the sample as in our uniaxial tests, the synthane end caps would not have presented any problem (8).

In addition to providing low confined modulus values, the synthane end caps and externally mounted displacement transducers also resulted in slightly lower ice strain rates.

Equations were derived to correct the extensometer readings (9). Triaxial tests were also performed on a synthane test specimen to determine the mechanical properties of the synthane and deformation characteristics of the triaxial cell. The results presented in

Table 1. Summary of force-displacement curve shapes for different strain rates, temperatures, and confining pressure/axial stress ratios.

	Number of tests for each curve type			
	Type A	Type B	Type C	Type D
-5°C (23°F)				
10^{-5} s^{-1} V, 0.25	5	2	3	0
10^{-5} s^{-1} V, 0.50	1	5	3	0
10^{-3} s^{-1} V, 0.50	8	0	1	0
-20°C (-4°F)				
10^{-3} s^{-1} V, 0.25	8	0	0	1
10^{-5} s^{-1} V, 0.50	3	2	4	0
10^{-3} s^{-1} V, 0.50	7	0	0	2

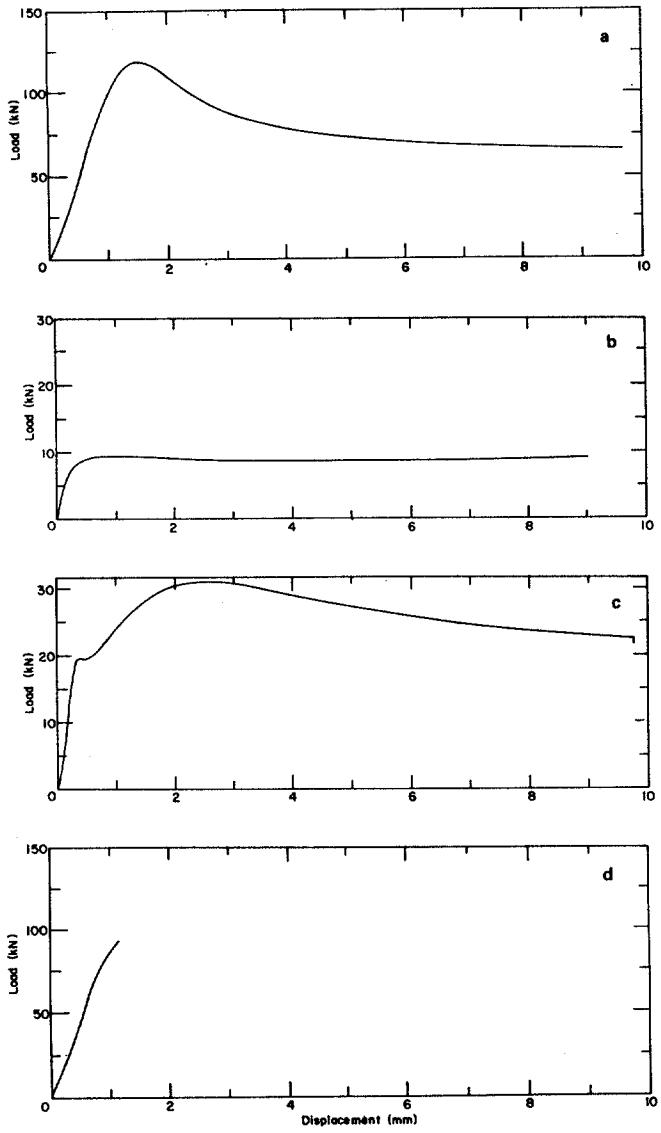

Fig. 4. Representative load-displacement curves observed during the tests.
a. Type A.
b. Type B.
c. Type C.
d. Type D.

Table 2 indicate that actual ice strain rates were up to 25% lower than the nominal strain rate. The greatest difference between the actual and nominal strain rates was found under test conditions where the ice was stiffest; that is, at high strain rate, low temperature, and high confining pressure.

Corrected confined modulus data were still too low. It was determined that initial strain and modulus measurements were also affected by closure at the loading piston-end cap interface. Closures less than 5.0 X 10^{-5} m were sufficient to reduce measured initial moduli by 50%. While it was possible to correct the test data and determine the average strain rate and failure strain for a given test, transducers in the cell are required to measure reliable initial tangent

Table 2. Mean average strain rates for each test condition.

	$\dot{\varepsilon}_n = 10^{-5}\ s^{-1}$	$\dot{\varepsilon}_n = 10^{-3}\ s^{-1}$
	$\sigma_3/\sigma_1 = 0.25$	
T = -5°C	$\dot{\varepsilon}_{avg} = 9.66 \times 10^{-6}\ s^{-1}$	-
T = -20°C	---	$\dot{\varepsilon}_{avg} = 7.88 \times 10^{-4}\ s^{-1}$
	$\sigma_3/\sigma_1 = 0.5$	
T = -5°C	$\dot{\varepsilon}_{avg} = 9.80 \times 10^{-6}\ s^{-1}$	$\dot{\varepsilon}_{avg} = 8.14 \times 10^{-4}\ s^{-1}$
T = -20°C	$\dot{\varepsilon}_{avg} = 9.73 \times 10^{-6}\ s^{-1}$	$\dot{\varepsilon}_{avg} = 7.43 \times 10^{-4}\ s^{-1}$

Table 3. Summary of confined strength data for different nominal strain rates, temperatures, and confining pressure/axial stress ratios.

	Confined Compressive Strength							
	Maximum		Minimum		Mean		Mean Porosity	
	(MPa)	(lbf/in.^{2})	(MPa)	(lbf/in.^{2})	(MPa)	(lbf/in.^{2})	(ppt)	Samples
-5°C (23°F)								
10^{-5} s^{-1} V, 0.25	3.95	573	1.14	166	2.86±0.98	415±142	79±17	10
10^{-5} s^{-1} V, 0.50	6.61	959	2.28	330	3.81±1.59	552±231	86±65	9
10^{-3} s^{-1} V, 0.50	17.94	2602	5.43	788	11.70±3.41	1697±495	78±39	9
-20°C (-4°F)								
10^{-3} s^{-1} V, 0.25	17.07	2475	11.58	1679	14.77±1.90	2141±275	77±42	9
10^{-5} s^{-1} V, 0.50	11.03	1600	3.95	573	6.59±1.97	956±286	82±39	9
10^{-3} s^{-1} V, 0.50	38.63	5602	8.34	1210	23.50±8.73	3408±1266	57±34	9

Table 4. Summary of confined failure strain data for different nominal strain rates, temperatures, and confining pressure/axial stress ratios. Data have been corrected for deformation of synthane end caps.

	Confined Failure Strain (%)				
	Maximum	Minimum	Mean	Mean Porosity (ppt)	Samples
-5°C (23°F)					
10^{-5} s^{-1} V, 0.25	0.97	0.35	0.70±0.25	79±17	10
10^{-5} s^{-1} V, 0.50	4.98	0.47	1.50±1.47	86±65	9
10^{-3} s^{-1} V, 0.50	0.87	0.24	0.42±0.19	78±39	9
-20°C (-4°F)					
10^{-3} s^{-1} V, 0.25	0.55	0.36	0.47±0.07	77±42	9
10^{-5} s^{-1} V, 0.50	4.97	0.59	1.86±1.79	82±39	9
10^{-3} s^{-1} V, 0.50	0.89	0.14	0.57±0.23	57±34	9

Table 5. Summary of confined time to failure data for different nominal strain rates, temperatures, and confining pressure/axial stress ratios.

	Confined Time to Failure (s)				
	Maximum	Minimum	Mean	Mean Porosity (ppt)	Samples
-5°C (23°F)					
10^{-5} s^{-1} V, 0.25	999	342	720± 259	79± 17	10
10^{-5} s^{-1} V, 0.50	>5000	540	1540± 1466	86± 65	9
10^{-3} s^{-1} V, 0.50	10.6	2.8	5.0± 2.3	78± 39	9
-20°C (-4°F)					
10^{-3} s^{-1} V, 0.25	7.2	4.6	6.0± 0.9	77± 42	9
10^{-5} s^{-1} V, 0.50	>5000	670	1908± 1777	82± 39	9
10^{-3} s^{-1} V, 0.50	12.0	2.0	7.2± 3.0	57± 34	9

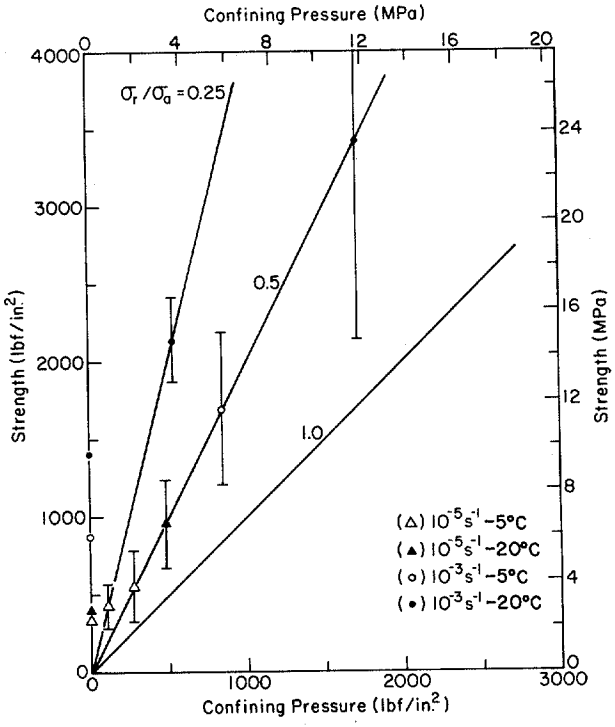

Fig. 5. Mean compressive strength versus confining pressure for multi-year pressure ridge samples at different temperatures and nominal strain rates.

modulus data (10). The confined initial tangent modulus data from the triaxial tests have therefore been rejected and are not presented in this paper.

Summaries of the strength and failure strain and the time to failure for each of the six test conditions are given in Tables 3, 4, and 5. The mean confined compressive strength of ice, σ_1, for each test condition is plotted against the confining pressure ($\sigma_2 = \sigma_3$) at failure in Fig. 5. Mean uniaxial compressive data are included for comparison (3). Strength data are also plotted against porosity (air plus brine volume) in Fig. 6. Ice porosities were calculated from the salinity, density, and temperature of each sample (11). A detailed tabulation of the test results can be found in Cox et al. (2).

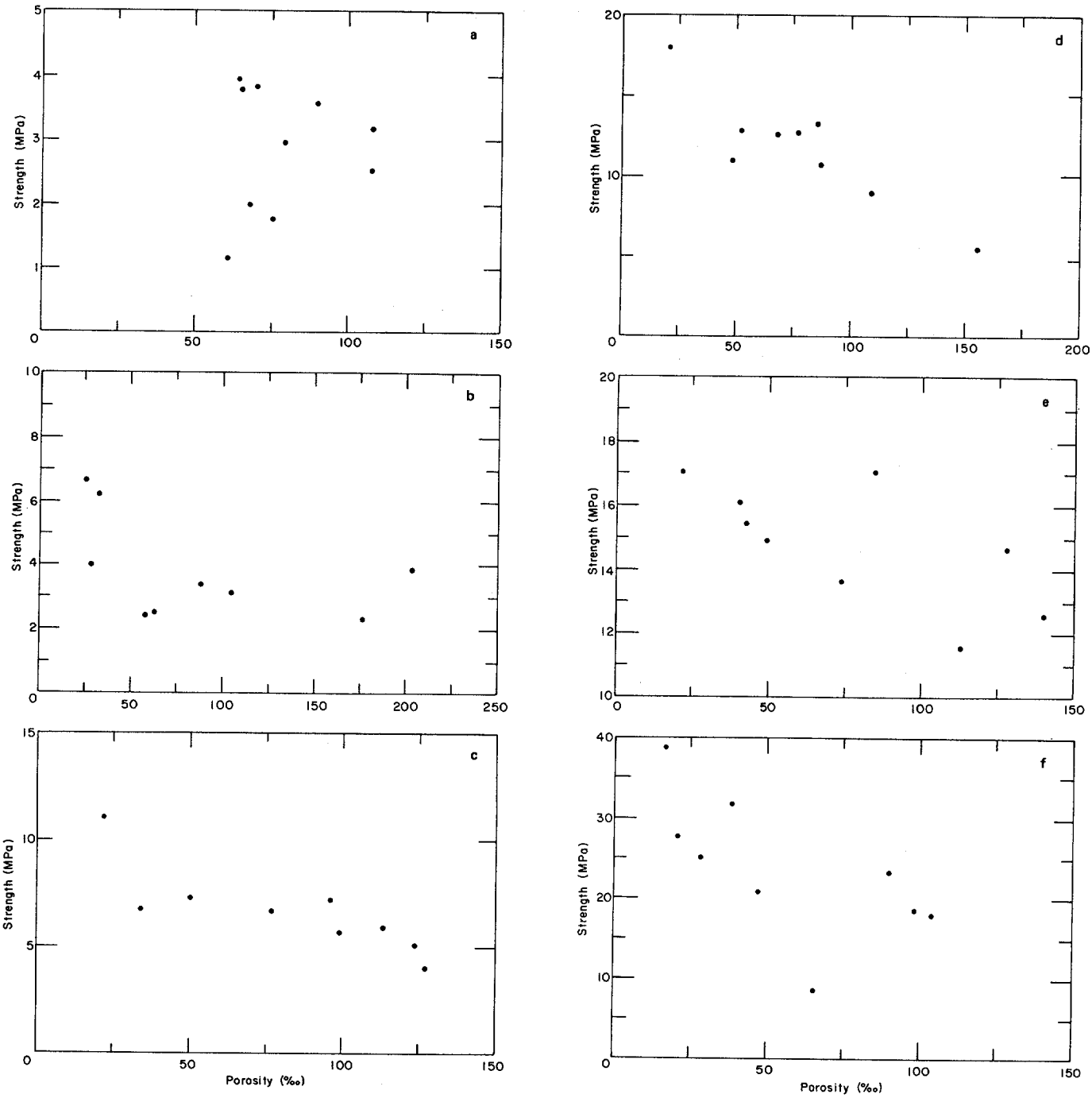

Fig. 6. Confined compressive strength versus ice porosity.

a. $\dot{\varepsilon} = 10^{-5}$ s^{-1}, T = -5°C, $\sigma_3/\sigma_1 = 0.25$.

b. $\dot{\varepsilon} = 10^{-5}$ s^{-1}, T = -5°C, $\sigma_3/\sigma_1 = 0.5$.

c. $\dot{\varepsilon} = 10^{-5}$ s^{-1}, T = -20°C, $\sigma_3/\sigma_1 = 0.5$.

d. $\dot{\varepsilon} = 10^{-3}$ s^{-1}, T = -5°C, $\sigma_3/\sigma_1 = 0.5$.

e. $\dot{\varepsilon} = 10^{-3}$ s^{-1}, T = -20°C, $\sigma_3/\sigma_1 = 0.25$.

f. $\dot{\varepsilon} = 10^{-3}$ s^{-1}, T = -20°C, $\sigma_3/\sigma_1 = 0.5$.

DISCUSSION

Load-Displacement Curves

Four types of load-displacement curves were observed in the tests and are designated as Types A, B, C, and D (Fig. 4, Table 1). In general, Type A behavior was the most common, where the sample first showed strain hardening, followed by some strain-softening, then plastic flow. This kind of behavior was found under all test conditions. Type B load-displacement curves, strain-hardening followed by plastic flow, was only observed at a nominal strain rate of 10^{-5} s^{-1} and was most common at a temperature of -5°C and a confinement axial stress ratio of 0.5. In Type C behavior, an initial yield point was observed in addition to the maximum stress or secondary yield point. According to Mellor and Cole (17), who tested freshwater polycrystalline ice, the initial yield point corresponds to the point at which internal cracks begin to form at a high rate. As with Mellor and Cole's experiment, two yield points were only observed at low strain rates (10^{-5} s^{-1}). At higher strain rates the initial yield point becomes dominant and the secondary yield point disappears (17). Type D behavior, no strain softening and rupture, was only observed at a nominal strain rate of 10^{-3} s^{-1} and a temperature of -20°C. The four kinds of load-displacement behaviour are consistent with our current understanding of the mechanical properties of polycrystalline ice (17).

Strength

For a given test condition the confined compressive strength is found to increase with decreasing temperature, increasing strain rate, and increasing confinement. In general these trends are consistent with triaxial test data for freshwater granular ice (14), laboratory-grown saline ice (15), and multi-year sea ice sheets (1). It appears that the confined compressive strength of vertical ice samples from multi-year ridges is less than that of multi-year sea ice sheets and laboratory-grown saline ice. Under comparable test conditions the confined compressive strength of ridge samples is about half that of multi-year sheet ice samples. This is not surprising as most of the multi-year sheet test specimens consisted of columnar grains that were loaded in the hard fail direction. The majority of the ridge ice samples in this study contained mixtures of granular ice and columnar fragments in various orientations.

It is interesting that the mean strength data for each temperature and strain rate follows the hydrostat ($\sigma_1 = \sigma_3$). In fact, the mean deviatoric yield stress ($\sigma_1 - \sigma_3$) shows little variation with confining pressure (σ_3) for all test conditions (Table 6). This suggests that it may be possible to represent multi-year pressure ridge ice as a Tresca material in ice-structure interaction models. However, the uniaxial compression data in Fig. 5 were obtained from ice samples having a much lower porosity than the triaxial specimens. If uniaxial specimens having a similar porosity had been tested, unconfined compressive strengths would have been lower than the deviatoric yield stress of the triaxial specimens. Consequently a Mohr- Cuolomb -- Tresca yield criteria as suggested by Coon et al. (16) for multi- year sheet ice may be more appropriate.

The confined compressive strength of multi-year pressure ridge ice samples also shows a strong tendency to decrease with increasing ice porosity (Fig. 6). The large scatter in the data is due to the variation in ice structure between the samples. Unusually strong or weak specimens for a given porosity generally contained a large proportion of columnar grains. Samples con-

Table 6. Mean deviatoric yield stress at different strain rates and temperatures.

$\dot{\varepsilon} = 10^{-5}$ s^{-1}, T = -5°C

$\overline{\sigma_1 - \sigma_3}$ (MPa)	$\overline{\sigma_3}$ (MPa)	$\overline{\eta}$ (ppt)
2.34±1.08	0	44
2.15±0.74	0.72±0.25	79
1.90±0.80	1.90±0.80	86

$\dot{\varepsilon} = 10^{-5}$ s^{-1}, T = -20°C

$\overline{\sigma_1 - \sigma_3}$ (MPa)	$\overline{\sigma_3}$ (MPa)	$\overline{\eta}$ (ppt)
2.79±0.79	0	36
3.29±0.99	3.29±0.99	82

$\dot{\varepsilon} = 10^{-3}$, T = -5°C

6.06±1.63	0	46
5.85±1.71	5.85±1.71	78

$\dot{\varepsilon} = 10^{-}$), T = -20°C

9.63±1.39	0	39
11.07±1.42	3.69±0.47	77
11.75±4.37	11.75±4.37	57

$\overline{\sigma_1 - \sigma_3}$ Mean deviatoric yield stress

$\overline{\sigma_3}$ Mean confining pressure

$\overline{\eta}$ Mean porosity (air and brine)

taining columnar grains oriented in a hard fail direction usually resulted in a high strength value, and samples containing columnar grains oriented in a soft fail direction resulted in low strength values. Similar observations have been made for uniaxial compression tests on multi-year ridge ice samples (5). A complete structural analysis of the triaxial test specimens is planned for the near future.

Failure Strain and Time to Failure

Mean failure strains and times to failure at the peak of maximum stress for each test condition are given in Table 4 and 5. As expected, confinement reduces cracking and causes the ice to be more ductile resulting in a larger strain at failure and time to failure. For those tests conducted at 10^{-3} s^{-1}, the failure strain and time to failure generally increase with the confined compressive strength. At 10^{-5} s^{-1}, due to the high plasticity of the ice, failure strains and times to failure are more variable and show no correlation with strength.

SUMMARY AND CONCLUSIONS

Fifty-five constant-strain-rate tests were performed on vertically oriented multi-year pressure ridge samples at different strain rates, temperatures, and confining pressures. Due to large variations in ice structure and porosity, the confined compressive strength data show considerable scatter. However, the confined compressive strength clearly increased with decreasing temperature, increasing strain rate, and increasing confining pressure. The results suggest that multi-year pressure ridge ice may be represented as a Tresca material. For a given strain rate and temperature, the deviatoric yield stress showed little variation with confining pressure. Confinement caused the ice to be more ductile and resulted in large failure strains.

REFERENCES

1. Cox, G.F.N., Richter-Menge, J.A., Weeks, W.F., Mellor, M. and Bosworth, H. "Mechanical properties of multi-year sea ice, Phase I: Test results," U.S. Army Cold Regions Research and Engineering Laboratory, Report 84-9, 105 p., 1984.

2. Cox, G.F.N., Richter-Menge, J.A., Weeks, W.F., Mellor, M., Bosworth, H., Durell, G. and Perron, N. "Mechanical properties of multi-year sea ice, Phase II: Test results," U.S. Army Cold Regions Research and Engineering Laboratory, in press.

3. Cox, G.F.N., Richter, J.A., Weeks, W.F., and Mellor, M. "A summary of the strength and modulus of ice samples from multi-year pressure ridges, "Proceedings, Third International Offshore Mechanics and Arctic Engineering Symposium, New Orleans, 1984, Vol. 3, pp. 126- 133. Journal of Energy Resources Technology, Vol. 107, pp. 93-98, March 1985.

4. Cox, G.F.N. and Richter-Menge, J.A. "Tensile strength of multi-year pressure ridge sea ice samples," Proceedings, Fourth International Offshore Mechanics and Arctic Engineering Symposium, Dallas, 1985, Vol. 2, pp. 186-193. Journal of Energy Resources Technology, in press.

5. Richter-Menge, J.A. and Cox, G.F.N. "The effect of sample orientation on the compressive strength of multi-year pressure ridge ice samples," Proceedings, ASCE Arctic '85 Conference, San Francisco, 1985, pp. 465-475.

6. Hawkes, I. and Mellor, M. "Uniaxial testing in rock mechanics laboratories." Engineering Geology, Vol. 4, 1970, pp. 177-285.

7. Schwarz, J., Frederking, R., Gavrillo, V., Petrov, I.G., Hirayama, K.I., Mellor, M., Tryde, P. and Vaudrey, K.D. "Standardized testing methods for measuring mechanical properties of ice." Cold Regions Science and Technology, Vol. 4, 1981, pp. 245-253.

8. Mellor, M., Cox, G.F.N. and Bosworth, H. "Mechanical properties of multi-year sea ice, testing techniques," U.S. Army Cold Regions Research and Engineering Laboratory, Report 84-8, 39 p., 1984.

9. Cox, G.F.N. and Richter-Menge, J.A. "Triaxial compression testing of ice," Proceedings, ASCE Arctic '85 Conference, San Francisco, 1985, pp. 476- 488.

10. Richter-Menge, J.A. "Static determination of Young's modulus in sea ice," Cold Regions Science and Technology, Vol. 9, No. 3, pp. 283-286, 1984.

11. Cox, G.F.N. and Weeks, W.F. "Equations for determining the gas and brine volumes in sea ice samples." Journal of Glaciology, Vol. 29, No. 2, pp. 306-316, 1983.

12. Richter, J.A. and Cox, G.F.N. "A preliminary examination of the effect of structure on the strength of ice samples from multi-year pressure ridges." Proceedings, Third International Offshore Mechanics and Arctic Engineering Symposium, New Orleasn, Vol. 3, pp. 140-144, 1984. Journal of Energy Resources Technology, Vol. 107, pp. 99-102, 1985.

13. Richter-Menge, J.A. and Cox, G.F.N. "Structure, salinity, and density of multi-year sea ice pressure ridges." Proceedings, Fourth International Offshore, Mechanics and Arctic Engineering Symposium, Dallas, 1985, Vol. 2, pp. 194-198. Journal of Energy Resources Technology, in press.

14. Jones, S.J. "The confined compressive strength of polycrystalline ice," Journal of Glaciology, Vol. 28, No. 98, pp. 171-177, 1982.

15. Nawwar, A.M., Nadreau, J.P. and Wang, Y.S. "Triaxial compressive strength of saline ice." Proceedings of the Seventh International Conference on Port and Ocean Engineering under Arctic Conditions, Helsinki, Finland, Vol. 3, pp. 193-201, 1983.

16. Coon, M.D., Evans, R.J., and Gibson, D.H. "Failure criteria for sea ice and loads resulting from crushing," Proceedings, IAHR Ice Problems Symposium, Hamburg, 1984, Vol. 3, pp. 1-16.

17. Mellor, M. and Cole, D.M. "Deformation and failure of ice under constant stress or constant strain rate," Cold Regions Science and Technology, Vol. 5, pp. 201-219, 1982.

ACKNOWLEDGEMENTS

This study was sponsored by Shell Development Company and the Minerals Management Service of the U.S. Department of the Interior, with support from Amoco Production Company, Exxon Production Research Company, and Sohio Petroleum Company.

The authors appreciate the assistance provided by Dr. W.F. Weeks in supervising the field sampling program, and the efforts of H. Bosworth, G. Durell, and N. Perron in preparing and testing the ice samples.

reprinted from

Proceedings of the Fifth (1986) International Offshore Mechanics and
Arctic Engineering OMAE Symposium – Volumn IV